BNL-108274-2015-JA

Controlled Surface Segregation Leading to Efficient Coke-Resistant Ni/Pt Bimetallic Catalysts for Dry Reforming of Methane

Lidong Li, Lu Zhou, Samy Ould-Chikh, Dalaver H. Anjum, Mohammed B. Kanoun, Jessica Scaranto, Mohamed N. Hedhili, Syed Khalid, Paco V. Laveille, Lawrence D'Souza and Jean-Marie Basset

Submitted to CHEMCATCHEM

March 2015

Photon Sciences Department

Brookhaven National Laboratory

U.S. Department of Energy
USDOE Office of Science,
Basic Energy Sciences

DISCLAIMER

Controlled Surface Segregation Leading to Efficient Coke-Resistant Ni/Pt Bimetallic Catalysts for Dry Reforming of Methane

*Lidong Li, Lu Zhou, Samy Ould-Chikh, Dalaver H. Anjum, Mohammed B. Kanoun, Jessica Scaranto, Mohamed N. Hedhili, Syed Khalid, Paco V. Laveille, Lawrence D'Souza and Jean-Marie Basset**

((Dedication----optional))

Reforming of natural gas with H_2O or CO_2 to produce syngas (i.e., CO and H_2), which is a key intermediate for production of many valuable chemicals and fuels such as ammonia, methanol, dimethyl ether and synfuel, represents one of major processes to utilize natural gas in industry. [1] Industrial reforming catalysts are principally based on nickel because of its low cost and high activity relative to noble metals. Nickel catalysts, however, readily induce coke formation, sintering and metal oxidation, leading ultimately to catalyst deactivation and plugging of a reactor, especially in CO_2 reforming. Compared to H_2O reforming, CO_2 reforming causes more severe coke formation due to the increased C/H molar ratio in the feedstock. Therefore, the development of a coke resistant nickel-based catalyst constitutes the major challenge for CO_2 reforming of methane.

The CO_2 reforming catalyst commonly consists of metal nanoparticle and oxide support. Although the reaction mechanism of CO_2 reforming is still under debate, it is generally accepted that CH_4 adsorbs and dissociates on the metal surface to yield the surface CH_x species and H_2, and the CH_x species further dehydrogenates to generate the adsorbed C*.[2] The C* nucleates and grows on the metal surface to form the graphite, which encapsulates the metal surface and finally leads to the deactivation of catalyst. CO_2 may react directly with the C* on the metal surface to generate CO via an Eley Rideal type mechanism (e.g., Rh catalyst[3]) or be activated by the reaction with the support via carbonate species (e.g., Pt/ZrO_2 [4]), which is dependent on the nature of metal and support. It is evident that the metal surface plays a crucial role in the CO_2 reforming catalytic circle. To inhibit or eliminate the coke formation, one of the practical routes is to prevent the C* nucleation and growth through modifying the metal surface. Nielsen *et al.*[5] have discovered that the ensemble size required for the carbon nucleation is larger than that needed for the reforming reaction. Based on this knowledge, they developed a carbon-free steam reforming of methane process (SPARG process) in which H_2S is added to the feedstock to suppress the ensemble size by partially poisoning the metal surface of nickel-based catalyst. The similar result has also been achieved in the Ni/TiO_2 catalyst system, in which the ensemble size of nickel particles can be modified by the mobile TiO_x species due to strong metal-support interaction (SMSI).[6] Both theoretical calculations and experimental studies have confirmed that the smaller the size of nickel particle is, the less the coke. [7] It is because the small size nickel particles can greatly impede the growth of the formed graphite. The recent studies have shown that the step sites might be the most active ones for carbon nucleation.[8] It means that blocking the step sites by some promoters (e.g., K[9] and Au[10]) can effectively suppress the carbon formation.

The other way to eliminate the coke formation is to enhance the gasification of carbon. It is well known that carbon formation is much less on noble metals than on nickel, which is mainly because the lower solubility of carbon in the noble metals favours the gasification of carbon. The addition of alkali (e.g., K_2O,[11,12] Na_2O[11]) or alkaline earth (e.g., MgO,[11] CaO[11]) metal oxides, as well as rare-earth metal oxides (e.g., La_2O_3 [13]), to promote nickel-based catalysts has been proved to be an efficient method to suppress the carbon formation, because the enhanced basicity of the supports may contribute to adsorption and dissociation of CO_2, which facilitates the gasification of carbon. The recent studies have shown that CeO_2 [14] and ZrO_2 [4, 15] as supports or promoters can effectively suppress the carbon formation because of their high oxygen storage capacities or excellent redox properties that can enhance the gasification of carbon.

The addition of secondary metals as promoters to primary catalysts (mainly nickel catalysts) is another efficient way to eliminate the carbon formation. A wide spectrum of metals (e.g., Fe, Co, Pt, Ag, Au, Mn, etc.) have to date been investigated.[16] The effects of secondary metals are diverse, which may function to reduce and stabilize the metal particle size of nickel catalysts (e.g., Pt,[17] Rh[18]), to tailor the ensemble size of nickel catalysts (e.g., Sn,[16c,19] Ag,[20] Au[10]), to block the step sites (e.g., K,[9] Au[10]), or to modify the surface electronic properties of nickel catalysts (e.g., Ge,[16c] Sn,[16c] Au[10]). However, most of these findings are based on theoretical calculations or limited structural evidences. The studies dedicated to the surface composition and structure of bimetallic catalysts, especially under reaction conditions, and their influences on CO_2 reforming reaction are scarce. However, these are of extreme importance in catalysis and are also hot topics in surface science. For instance, in the case of Ni/Pt bimetallic systems, the

[*] Dr. L. Li, Dr. L. Zhou, Dr. S. Ould-Chikh, Dr. M. B. Kanoun, Dr. P. V. Laveille and Prof. J.-M. Basset
KAUST Catalysis Center (KCC)
King Abdullah University of Science & Technology
Thuwal 23955-6900 (Saudi Arabia)
E-mail: jeanmarie.basset@kaust.edu.sa
Dr. S. Khalid
Brookhaven National Laboratory
Upton, New York 11973-5000
United States
Dr. D. H. Anjum, Dr. M. N. Hedhili
Core Lab
King Abdullah University of Science & Technology
Thuwal 23955-6900 (Saudi Arabia)
Dr. L. D'Souza and Dr J. Scaranto
SABIC Corporate Research and Innovation Center
Saudi Basic Industries Corporation
Thuwal 23955-6900 (Saudi Arabia)

[**] We appreciate Saudi Basic Industries Corporation (SABIC) for financial support. We gratefully thank Dr. Elodie Guyonnet and Dr. Janet C. Mohandas for the helpful discussion.

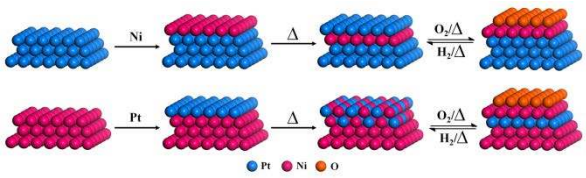

Scheme 1. Surface restructuring of Ni/Pt bimetallic systems induced by temperature and adsorbates.

surface is known to vary as a function of temperature and adsorbates, as schematically represented in Scheme 1. Ni atoms can deposit on the Pt surface to form a Ni monolayer, e.g., Ni/Pt(111).[21] Upon annealing at high temperature, Ni atoms diffuse into the subsurface region of Pt, leading to stable Pt−Ni−Pt(hkl) structure,[21–23] whereas, in the presence of O_2, they segregate to the surface, resulting in O/Ni−Pt−Pt(hkl) structure.[22– 26] Correspondingly, their catalytic properties (e.g., hydrogenation and oxygen reduction reaction) vary with bimetallic surface.[21–24] Conversely, Pt atoms can deposit on the Ni surface to generate a Pt monolayer, e.g., Pt/Ni(111),[27,28] which transforms into a surface alloy upon annealing. In the presence of O_2, Ni atoms segregate to the surface, leading to O/Ni−Pt−Ni(hkl) structure.[25,26] The similar phenomena have also been observed on other bimetallic systems such as Cu/Ni, [29] Pt/Co [30] and Ni/Cr [31] systems. It is evident that the structure of bimetallic surface is very flexible, remarkably varying with the reaction conditions, which in turn modifies the catalytic properties.[21–24,32]

Nonetheless, most of these insights regarding bimetallic surface segregation are obtained from model bimetallic surface under ultrahigh vacuum (UHV) environment or theoretical calculation. To convert these knowledge into a practical industrial catalysts, in which the active metal is present in the form of nanoparticle (NP) anchored on a high-surface-area support is limited by the availability of bimetallic catalysts with controlled surface composition and structure, which is hard to be achieved by the conventional methods (e.g., impregnation or precipitation). The latter leads very often to the additional formation of monometallic NPs on the supports. To tackle this issue, a facile method to prepare "pure" supported Ni/Pt bimetallic NPs with controlled surface composition and structure was developed in this work. The method is based on preferential reduction of Pt precursor (e.g., $Pt(acac)_2$) by surface nickel hydrides (Ni_s–H) that are generated by treatment of as-prepared Ni NPs under hydrogen flow at 450 ºC. It finally leads to a monolayer of metallic Pt atoms deposited on the surface of Ni NPs. The preparation is detailed in our recent patent.[33] To assess the surface and bulk structure according to the Pt/Ni elemental composition, a series of alumina-supported Ni/Pt bimetallic NPs with various Pt coverage, denoted as $NiPt(X)/Al_2O_3$ (X= 0.18–0.71) where X is molar ratio of the Pt atoms to the surface Ni atoms (assuming in a first approximation that the Ni NPs remain intact during preparation of the bimetallic NPs), were prepared and characterized using infrared spectroscopy of adsorbed carbon monoxide (CO-IR), aberration corrected high-angle annular dark-field scanning transmission electron microscopy (HAADF-STEM), energy-dispersive X-ray spectroscopy (EDX), extended X-ray absorption fine structure (EXAFS), X-ray absorption near edge structure (XANES) techniques, X-ray diffraction (XRD) and X-ray photoelectron spectroscopy (XPS). The monometallic Ni and Pt NPs were also synthesized for comparison. As discussed above, surface segregation, presumably induced by temperature and adsorbates, has a marked effect on the catalytic properties of bimetallic catalysts. Therefore, it is practically important to study surface segregation of our bimetallic NPs under reaction conditions. To this end, the Ni/Pt bimetallic samples were treated at 700 ºC under vacuum for 1 h to simulate the catalytic conditions. All the samples were characterized by various techniques before and after thermal treatment. The catalytic tests show that these bimetallic NPs are active catalysts for CO_2 reforming of methane, and their catalytic activities and stabilities, as well as coke formation, noticeably vary as a function of the Pt coverage. Relationships of structures and catalytic properties of these bimetallic catalysts were investigated.

Table 1. Textural properties of the monometallic and bimetallic catalysts.

Samples	Ni (wt%)	Pt (wt%)	M_s[a] (mmol/g Cat)	Pt/Ni_s[b]	d[c] (nm)	d[d] (nm)
Ni/Al_2O_3	10.0	–	0.24	–	6.9	–
Pt/Al_2O_3	–	3.0	0.11	–	1.4	–
$NiPt(0.18)/Al_2O_3$	9.14	0.75	0.25	0.18	7.1	7.4
$NiPt(0.66)/Al_2O_3$	9.38	2.91	0.27	0.66	7.2	7.2
$NiPt(0.71)/Al_2O_3$	8.83	2.93	0.25	0.71	7.5	7.9

[a] M_s refers to the amount of the surface metal atoms, determined by H_2–O_2 titration. [b] Pt/Ni_s refers to the molar ratio of the Pt atoms to the surface Ni atoms, assuming in a first approximation that the Ni NPs remain intact during preparation of the bimetallic NPs. [c] and [d] *d* refers to particle sizes, determined by (S)TEM before and after thermal treatment at 700 ºC under vacuum for 1 h, respectively.

The properties of all the monometallic and bimetallic samples are summarized in Table 1 and Figure S6 (Supporting Information). The total metal loading of bimetallic samples vary within 10–12 wt%, which is comparable to the monometallic Ni sample (10 wt%). The metal nanoparticle sizes of bimetallic samples (7.1–7.5 nm) are slightly larger than that of the monometallic Ni sample (6.9 nm). The amounts of surface metal atoms for the monometallic Ni and bimetallic samples measured by H_2-O_2 titration are comparable (0.24–0.27 mmol/g Cat). The thermal treatment at 700 ºC under vacuum for 1 h has an insignificant effect on the metal nanoparticle sizes of bimetallic samples, as shown in Table 1 and Figure 6S.

Figure 1 presents IR spectra of CO adsorbed on various samples before and after thermal treatment. As shown in Figure 1a, the CO absorption bands on pure Ni and Pt NPs are strikingly different. For the Ni NPs, two main absorption bands at 2037 and 1942 cm^{-1} are assigned to linear Ni–CO and bridged $Ni_2(\mu$-CO) species, respectively.[34] For the Pt NPs, two absorption bands at 2065 and 1810 cm^{-1} were observed, which are ascribed to linear Pt–CO and bridged $Pt_x(\mu$-CO) (x= 2,3) species, respectively, and the former is very intense whereas the latter is noticeably weaker.[35] As the Pt atoms are deposited on the Ni surface to generate bimetallic NPs, the band corresponding to linear Ni–CO species is markedly suppressed and the newly-formed band at ca. 2065 cm^{-1}, being assigned to linear Pt–CO species, dominates the absorption bands and its intensity increases proportionally with the Pt coverage. Such vibrations are characteristic of CO adsorbed on Pt-enriched Ni surface.[36] In the meantime, the absorption band corresponding to bridged $Ni_2(\mu$-CO) species decreases remarkably with the Pt coverage and shifts to lower frequency, accompanied by the broadening of the absorption peak.

Upon thermal treatment, the IR spectra of adsorbed CO vary greatly, as shown in Figure 1b for $NiPt(0.71)/Al_2O_3$. The absorption band for bridged $Ni_2(\mu$-CO) species remarkably increases and shifts to higher frequency, while the band for linear Pt–CO species has no significant shift and just its relative intensity decreases. In the meantime, a high frequency absorption band at ca. 2115 cm^{-1} and a

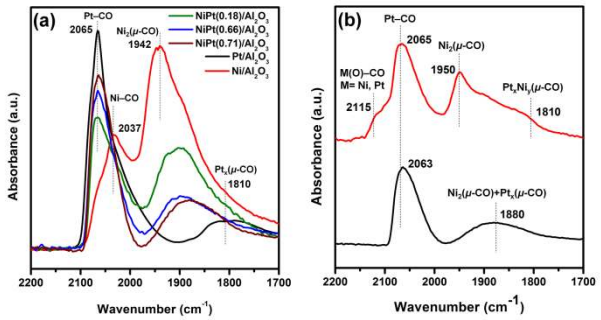

Figure 1. (a) IR spectra of CO adsorbed on alumina-supported Ni and Pt monometallic or bimetallic NPs before thermal treatment and (b) comparison of IR spectra of CO adsorbed on NiPt(0.71)/Al_2O_3 before (black line) and after (red line) thermal treatment.

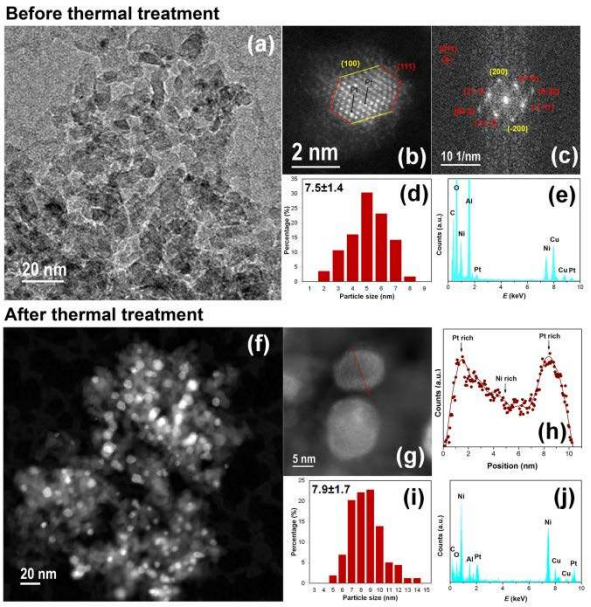

Figure 2. Typical (S)TEM images of NiPt(0.71)/Al_2O_3 (a) before and (f) after thermal treatment. (b), (c) and (e) HAADF-STEM image, the corresponding indexed fast Fourier transform (FFT) and EDX spectra of a selected single nanocrystal of untreated NiPt(0.71)/Al_2O_3. (d) and (i) Particle size distributions of NiPt(0.71)/Al_2O_3 before and after thermal treatment, respectively. (g), (h) and (j) HAADF-STEM image, compositional line profile and EDX spectra of a selected NP of treated NiPt(0.71)/Al_2O_3.

low frequency band at ca. 1810 cm^{-1} are present. The similar results were observed for the other bimetallic samples (Figure S7 in Supporting Information). The low frequency band at ca. 1810 cm^{-1} corresponds to the bridged species, e.g., Pt$_x$(μ-CO) (x= 2,3)[35] and Ni$_x$(μ-CO) (x= 3,4).[34] However, because thermal treatment leads to the formation of surface alloy with low Pt–Pt coordination number for our bimetallic samples (see EXAFS below), this band is very likely related to a bridged species Pt$_x$Ni$_y$(μ-CO) (x+y= 2–4). For the shoulder band at ca. 2115 cm^{-1}, its frequency is higher than those of linear species of CO adsorbed on the Pt or Ni surface (2030–2070 cm^{-1} for Ni–CO,[34] and 2040–2090 cm^{-1} for Pt–CO[35]) and lower than those of CO adsorbed on metal cations (e.g., 2186 cm^{-1} for Al^{3+}–CO,[37,38] 2195 cm^{-1} for Ni^{2+}–CO,[34,38] 2161 cm^{-1} for Pt^{2+}–CO[37,38]). Raskó[39] observed a band at 2112 cm^{-1}, which is quite close to the band of 2115 cm^{-1}, in the cases of Pt/TiO_2, Pt/SiO_2 and Pt/Al_2O_3, and assigned this band to CO adsorbed on the monoatomic Pt^0 that is generated by disruption of Pt crystallite into Pt^0 atoms with the help of CO. It can however be ruled out in our case since we did not observe the same band on the untreated samples. Primet *et al.*[40] observed a band at 2120 cm^{-1} when O_2 is adsorbed on a CO covered Pt surface or CO is adsorbed on an O_2 covered Pt surface, and assigned this band to a species Pt(O)–CO. Considering the possible strong interaction induced at high temperature of the metallic atoms with the oxygen atoms of the support at the NPs/support perimeter, the 2115 cm^{-1} band is tentatively assigned to the species M(O)–CO (M= Ni or Pt). It is evident from CO-IR spectra that the surface of the bimetallic NPs rearranges upon thermal treatment. The Pt atoms on the NP surface are partially exchanged with the Ni atoms, thus leading to an increase of nickel surface composition after thermal treatment. Similar behaviours were also observed for the samples treated at 450 ºC under vacuum for 1 h, implying that surface restructuring may take place at even lower temperature.

Figure 2 displays the typical STEM and HRTEM images of NiPt(0.71)/Al_2O_3 before and after thermal treatment. The similar images were also observed for NiPt(0.18)/Al_2O_3 and NiPt(0.66)/Al_2O_3 (see Figures S8 and S9 in Supporting Information, respectively). For the untreated samples, EDX analyses of tens of individual particles for each sample revealed no monometallic Ni or Pt particles, which prove the advantage of our preparation protocol to synthesize "pure" bimetallic NPs. A typical EDX spectrum for the selected single nanocrystal of NiPt(0.71)/Al_2O_3 is shown in Figure 2e. The detectable interplanar distances (d{111}= 1.94–2.05 Å and d{002}= 1.70–1.80 Å) characteristic on a regular face-centered cubic (fcc) nickel crystal imply that the Ni NPs remain unchanged during the preparation. It can also be observed in Figures 2b and 2c that, the exposed surfaces mainly consist of the {111} and {100} facets, being consistent with those expected from the truncated cuboctahedron model for the fcc metal NPs (e.g., Ni and Pt).[41] Since the brightness is proportional to the square of atomic number Z of an element on the STEM images, the Pt atoms are much brighter than Ni atoms owing to its larger atomic number. It can be clearly observed in Figure 2b that the brighter Pt atoms are well dispersed on the Ni surface in an atomic pattern. For the treated samples, it is apparent that the thermal treatment has no significant effects on the particle sizes, as observed in Figures 2d and 2i (and also in Figures S8 and S9 in Supporting Information). The same EDX analyses ruled out the presence of the monometallic Ni or Pt NPs. Figure 2j shows a typical EDX spectrum for the selected NP of NiPt(0.71)/Al_2O_3. It can be seen from Figures 2f and 2g that all the bimetallic NPs are partially covered with "thin and brighter" outmost layers. The compositional line profile analysis depicted in Figure 2h demonstrates that these outmost layers are Pt-enriched.

Figure 3 presents the XRD patterns of the bimetallic samples before and after thermal treatment and after dry reforming tests. Before thermal treatment, for all the bimetallic samples the diffraction peaks characteristic for the fcc nickel NPs (44.4° for Ni(111) and 51.7° for Ni(200), respectively)[42] are hardly detected, presumably due to the small nickel nanoparticle size or overlap with the diffraction peaks of γ-Al_2O_3. No peaks for the monometallic Pt NPs are observed. After thermal treatment and dry reforming reaction, a new diffraction peak appears, which falls in between 44.4° (Ni(111)) and 39.8° (Pt(111)),[43] and shifts to lower 2θ values with the increase of the initial Pt coverage from NiPt(0.18)/Al_2O_3, NiPt(0.66)/Al_2O_3 to NiPt(0.71)/Al_2O_3, suggesting the formation of Ni/Pt alloy.

In order to gain more insight into the structures of the bimetallic samples before and after thermal treatment, X-ray absorption spectroscopy (XAS) were carried out on the samples. Figure 4 schematically presents the typical Fourier transforms of the Pt L_3-

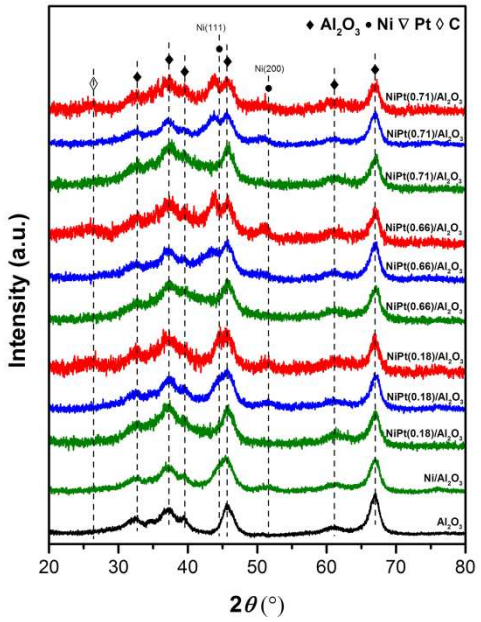

Figure 3. Comparison of XRD patterns of monometallic and bimetallic samples before (olive) and after (blue) thermal treatment at 700 ºC under vacuum for 1 h and after the dry reforming tests at 700 ºC (red).

edge k_2-weighted EXAFS signal for NiPt(0.71)/Al_2O_3 before and after thermal treatment and the corresponding back Fourier transforms. The fit results for all the samples are given in Table 2. It can be seen from Table 2 that, before thermal treatment, the first coordination spheres of Pt atoms for three bimetallic samples are well fitted with ca. 3 Ni atoms (Pt–Ni bond distance, 2.547–2.556 Å) and ca. 4 Pt atoms (Pt–Pt bond distance, 2.677–2.700 Å). The variation of Pt coverage has almost no effect on the first coordination sphere. The average coordination number (determined by EXAFS) is dependent on the size and shape of the metal NPs,[44] as well as segregation for the bimetallic NPs.[45] The smaller the size of the metal NPs, the lower the average coordination number because of the high proportion of low-coordinated surface atoms.[44] The formation of very small Pt clusters (<1 nm) on alumina with the corresponding Pt–Pt coordination number (N(Pt–Pt)=4.8) is first excluded because those were not observed by the (S)TEM. The total coordination number of the Pt atom for all the bimetallic samples is ca. 8. If the Pt atoms were dispersed homogenously into the synthesized 7 nm nickel NPs, the theoretical coordination number is around 11.[44a] This large difference implies that the Pt atoms locate on the surface of the Ni NPs, which is in accordance with the (S)TEM and CO-IR results. Considering that the {111} and {100} planes are the most exposed facets for the Ni NPs as observed in the (S)TEM, we calculated the coordination number of Pt atom on each facet assuming that the Pt atoms deposit as a monolayer (see Figure S10 in Supporting Information). It can be seen that the coordination numbers of the Pt atoms for all the bimetallic samples match well with those obtained from the {111} and {100} facets if the possible decrease of N(Pt–Pt) due to the incomplete coverage is considered. On the other hand, it can be found that, for all the untreated bimetallic samples, their Pt–Ni and Pt–Pt bond distances vary in very narrow ranges of 2.547–2.556 Å and 2.677–2.700 Å, respectively. The former are longer than the Ni–Ni bond in the metallic Ni (2.49 Å),[46] while the latter are largely shorter than the Pt–Pt bond in the metallic Pt (2.78 Å),[46] probably because of the constraints that the Ni surface lattice applies to the Pt monolayer.

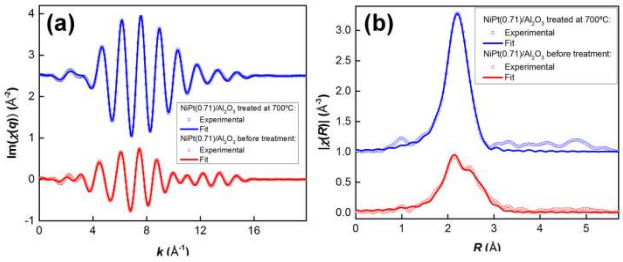

Figure 4. Imaginary part of the back Fourier transform (a) and Fourier transforms (b) of the EXAFS k^2-weighted $\chi(k)$ functions for NiPt(0.71)/Al_2O_3 before and after thermal treatment at 700°C under vacuum for 1 h. The empty squares are the experimental data while the solid lines are the fit results conducted within a k-range between 2.2 and 14.7 Å^{-1} and within an R-range of 1.2 up to 3.1 Å.

Table 2. Parameters extracted from the fits of EXAFS data.

Sample	Bond	N[a]	R (Å)	σ^2[b]
NiPt(0.18)/Al_2O_3	Pt–Ni[c]	3.4±0.3	2.547±0.007	7.7±0.5
	Pt–Pt[c]	4.1±0.4	2.677±0.006	10.2±0.7
	Pt–Ni[d]	10.6±0.6	2.55±0.01	5.9±0.4
	Pt–Pt[d]	–	–	–
NiPt(0.66)/Al_2O_3	Pt–Ni[c]	3.5±0.3	2.549±0.005	7.5±0.5
	Pt–Pt[c]	4.1±0.4	2.687±0.005	10.3±0.6
	Pt–Ni[d]	6.5±0.3	2.547±0.003	6.4±0.3
	Pt–Pt[d]	1.9±0.6	2.67±0.01	6±1
NiPt(0.71)/Al_2O_3	Pt–Ni[c]	3.3±0.3	2.556±0.005	7.4±0.4
	Pt–Pt[c]	4.8±0.4	2.700±0.004	9.9±0.6
	Pt–Ni[d]	6.9±0.4	2.545±0.003	6.3±0.3
	Pt–Pt[d]	1.5±0.5	2.66±0.02	5±1
Pt foil	Pt–Pt	12	2.76±0.01	2±1

[a] N refers to coordination number. [b] in10^{-3} Å^2. [c] Before thermal treatment. [d] After thermal treatment. For all the samples, ΔE_0 varies in the range of 3.7–8.4 eV and R-factor varies in the range of 0.01–0.02.

Upon thermal treatment, the first coordination sphere of the Pt atom is substantially modified as shown in Table 2. The N(Pt–Ni) increases from ca. 3 to ca. 7 while the N(Pt–Pt) correspondingly decreases from ca. 4 to ca. 2, the total coordination number being still ca. 8. Since the total coordination number is still much lower than the theoretical one (ca. 11) for the metal NPs with comparable particle size, except NiPt(0.18)/Al_2O_3, it implies that, after thermal treatment, the Pt atoms remain on the surface/subsurface of the bimetallic NPs, which is in agreement with those observed in the (S)TEM and CO-IR spectra. However, the marked variation of N(Pt–Ni) and N(Pt–Pt) unambiguously indicates that surface restructuring takes place upon thermal treatment. Considering the increase of the Ni composition in the surface after thermal treatment, as observed in the CO-IR spectra, it can be imagined that the Pt atoms on the surface of the Ni NPs diffuse into the sublayers to form the surface alloy upon the thermal treatment, while the Ni atoms in the sublayers migrate into the outer layer, finally leading to the increase of N(Pt–Ni) and the decrease of N(Pt–Pt). This observation is also in accordance with the overall decrease of the Dybye-Waller factors and the Pt–Pt distance after thermal treatment, which is expected when the Pt atoms sit in a crystallographic position within

the Ni crystal lattices (see Table 2). For the particular case of NiPt(0.18)/Al_2O_3, no Pt-Pt scattering paths could be detected and the coordination number of the Pt-Ni bond is around 11. It suggests

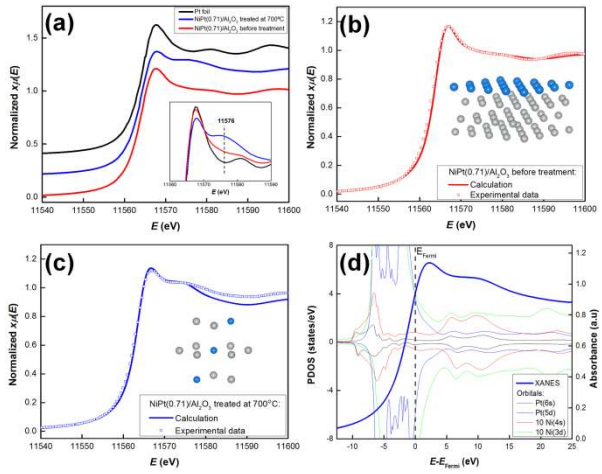

Figure 5. (a) Normalized Pt L_3-edge XANES spectra of a Pt foil and NiPt(0.71)/Al_2O_3 before and after thermal treatment at 700°C under vacuum for 1 h. The inset is a magnification of the energy range near the absorption edge. (b) Calculated spectra with FDMNES code assuming that the Pt atoms deposit as an epitaxial monolayer on the {111} planes of the Ni NPs with average particle size of 7 Å and (c) assuming that one Pt atom substitutes one Ni atom in a Ni crystal. (d) Overlap of the previous calculated spectra with the corresponding projected density of states on the central Pt atom and the surrounding Ni atoms.

that the proportion of Pt atoms reaching the bulk of Ni crystal is higher when the initial Pt coverage is lower.

The in-depth analysis of the XANES spectra of NiPt(0.71)/Al_2O_3 further substantiates the findings obtained from the EXAFS. The XANES results are schematically presented in Figure 5. As displayed in Figure 5a, the Pt foil shows the most intense white line at ca. 11567 eV. For the untreated NiPt(0.71)/Al_2O_3 (*N*(Pt–Ni)= 3.3), the intensity of the white line slightly drops with respect to that of the Pt foil, and it further decreases when the NiPt(0.71)/Al_2O_3 was treated at high temperature (*N*(Pt–Ni)= 6.9). The intensity of the white line appears to be a function of the Ni content in the first coordination sphere of the Pt atoms. This observation is consistent with the results of the previous studies,[47] especially that conducted by Moraweck *et al.*.[47a] They investigated the alloying effects on X-ray absorption edges (Pt L_2 and L_3 edge and Ni K edge) of a series of Ni_xPt_{1-x} single crystals, and concluded that an electron transfer from Ni to Pt occurs and results in a progressive filling of the Pt 5d band as the Ni content is increased. Since the Pt L_3 near edge structure corresponds to $2p_{3/2} \rightarrow 5d_{3/2}$ and $5d_{5/2}$ allowed transitions, and the probability of transition per unit time is proportional to the density of the final states (Fermi golden rule), it has been concluded that the state depletion just above the Fermi level due to the electron transfer from Ni to Pt can explain the variation of the white line intensity. However, Choi *et al.* [48] observed using X-ray photoelectron spectroscopy that the electron transfer in Ni_xPt_{1-x} alloys is in general very small, which is contradictory with the findings of Moraweck *et al.*[47a] It is also worth noting that a shoulder band (ca. 11576 eV) next to the white line is observed, which varies in intensity as a function of the surface composition (see inset in Figure 5a). This transition has also been observed, although not mentioned, in the Moraweck's work,[47a] in which this band enhances with the Ni content in the Ni_xPt_{1-x} alloy.

To elucidate such effects, we investigated the electronic structure of Ni/Pt bimetallic systems using the first principles calculation within the density functional theory. The Ni_xPt_{1-x}

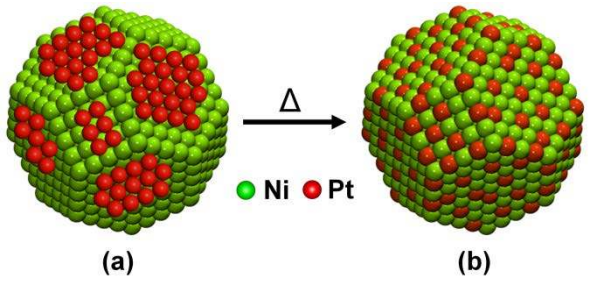

Scheme 2. Evolution of surface structure of the Ni/Pt bimetallic NPs upon thermal treatment.

systems were modelled with two supercells built of 2×2×2 containing eight conventional cells. In the first supercell, the Ni atom in the centre of the cell was substituted by one Pt atom, while in the second the atoms in the first coordination shell of the central Pt were replaced by 12 Pt atoms. The details of calculations and site-projected partial density of states plots (see Figure S5) are given in Supporting Information. The charge transfer from Ni to Pt was found to be very small in our calculation. When the Ni atoms are present in its first coordination sphere, the densities of states of the Pt d-orbitals near the Fermi level are indeed reduced, explaining the decrease of the white line intensity. In the meantime, new states located between 5 to 10 eV above the Fermi level appear and are composed of Pt(5d-6s) and Ni(3d-4s) orbitals, which could explain the new transition observed at 11576 eV. The depletion near the Fermi level seems to be due to a different hybridisation scheme of the Pt empty orbitals with the surrounding Ni empty orbitals rather than a Ni→Pt charge transfer.

Thus, theoretical XANES spectra were also calculated using the FDMNES code for two model clusters derived from the above EXAFS fits of NiPt(0.71)/Al_2O_3 before and after thermal treatment: the Pt atoms depositing as a monolayer on the Ni {111} plane and one Pt atom locating in the centre of a Ni crystal by replacing the central Ni atom. For the latter model, the first coordination shell of the central Pt atom was tuned by substituting two Ni atoms with two Pt atoms. Both calculations show excellent agreements with the experimental data (see Figures 5b and c). A calculation using a cluster with Pt atoms deposited as a monolayer on the Ni {100} plane also gives a fairly good agreement. The theoretical spectra reproduce the intensity of the white line and the shoulder at 11576 eV, both being confirmed to vary with Ni content in the first coordination sphere. The analysis of the projected density of states calculated with FDMNES (see Figure 5d) shows that the transition at 11576 eV arises from the availability of new empty states composed of Pt and Ni d-orbitals in accordance with the calculations operated with WIEN2K.

Combining all the findings obtained from the CO-IR, (S)TEM, XRD, EXAFS and XANES, one can find the following experimental facts. For the untreated samples, the Ni NPs remains unchanged during the preparation and the Pt atoms deposit on the surface of the Ni NPs, as demonstrated by the (S)TEM and CO-IR spectra. The EXAFS fittings and XANES simulation further confirm that the Pt atoms locate on the surface of the bimetallic NPs, and

most probably exist as a monolayer. Based on these facts and the consideration of the incomplete Pt coverage for all the bimetallic samples, a structure model for the untreated bimetallic samples can be proposed, as presented in Scheme 2a, in which the Pt atoms deposit on the surface of the Ni NPs as a monolayer islands. For the

Table 3. Summary of catalytic tests for CO_2 reforming of methane.[a]

Catalyst	Amount (mg)	5 min			20 h			rate(C)[d]
		X(CH_4) (%)[b]	TOF of CH_4[c]	H_2/CO	X(CH_4) (%)[b]	TOF of CH_4[c]	H_2/CO	
Ni/Al_2O_3	10	14.1	1.43	0.72	6.1	0.62	0.60	5.2
$NiPt(0.18)/Al_2O_3$	10	17.5	1.71	0.68	7.6	0.75	0.52	4.9
$NiPt(0.66)/Al_2O_3$	10	18.2	1.78	0.63	9.2	0.90	0.47	2.2
$NiPt(0.71)/Al_2O_3$	10	20.5	2.01	0.66	10.2	1.00	0.47	1.1
Pt/Al_2O_3	20	22.1	2.45	0.73	5.8	0.64	0.69	0.6

[a] General reaction conditions: *P*= 1 atm, *T*= 600 ºC, *t*= 20.0 h, $CH_4/CO_2/N_2$= 1:1:8, *flow rate*= 100 ml min^{-1}. [b] X(CH_4) refers to the conversion of CH_4. [c] In 10^3 mol CH_4 mol surface $metal^{-1}$ h^{-1}. [d] Rate(C) refers to the rate of carbon formation, in mol C mol surface $metal^{-1}$ h^{-1}.

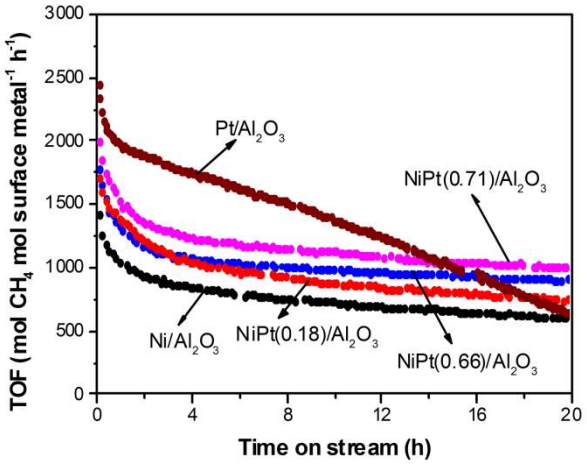

Figure 6. Comparison of the catalytic activities of the monometallic and bimetallic catalysts for CO_2 reforming of methane conducted at 600 ºC.

treated samples, the Pt atoms still locate on the surface of the bimetallic NPs, as revealed by the CO-IR, (S)TEM and EXAFS. The XRD patterns indicate the presence of Ni/Pt alloy, which is consistent with the XANES simulation. Based on these facts, a structure model composed of Ni-rich core and Ni/Pt alloy shell can be proposed, as shown in Scheme 2b.

All the monometallic and bimetallic NPs synthesized in this work were tested as catalysts for dry reforming of methane at moderate temperature (600 ºC) and high space velocity (600 L h^{-1} g cat^{-1}, except 300 L h^{-1} g cat^{-1} for Pt/Al_2O_3). These conditions make the reactions operate away from the thermodynamic equilibrium. The turnover frequency (normalized by surface metal atoms) is used to express the catalytic activity. The catalytic tests show that all the bimetallic NPs, as well as the monometallic samples, are active catalysts for CO_2 reforming of methane. The results are given in Fig. 6 and Table 3. For the two monometallic catalysts, Pt/Al_2O_3 is remarkably more active than Ni/Al_2O_3, which is consistent with other groups' work,[49] and is mainly determined by the nature of metal. Additionally, the small nanoparticle sizes of Pt/Al_2O_3 may also partially contribute to its high activity because the small particle sizes may lead to more step sites on the metal surface that are more active than the facet sites.[8a] Both Pt/Al_2O_3 and Ni/Al_2O_3 however deactivate rapidly with reaction time. For the former, its deactivation results mainly from the sintering because the particle sizes increase almost by 2 times after the reforming reaction (see Figure S6 in Supporting Information), while for the latter, its deactivation is ascribed mainly to the carbon formation because the particle sizes remain nearly unchanged after the reforming reaction (see Figure S6 in Supporting Information), but a large amount of carbon was formed (see Table 3). For all the bimetallic catalysts, they show high initial activities, and deactivate rapidly during the first 4 h, and then become relatively stable until 20 h. Their catalytic activities vary as a function of the Pt coverage. As the Pt coverage rises, their activities increase. All the bimetallic catalysts are more active than Ni/Al_2O_3, but less active than Pt/Al_2O_3. For the carbon formation, an opposite trends are observed, as shown in Table 3. The rate of carbon formation decreases with increasing the Pt coverage. The same tendency has also been observed for the dry reforming operated at 700 ºC, as shown in Figure S11 and Table S3. The CH_4 conversion increases with increasing the Pt coverage and the reaction reaches the thermodynamic equilibrium at 0.71 of the Pt coverage, while the carbon formation decreases as the Pt coverage increase. Since the metal loading and nanoparticle sizes for all the bimetallic catalysts are comparable, the differences of their catalytic performances can be ascribed to their varied surface structure and composition.

Actually, Ni/Pt bimetallic systems have been widely investigated for CO_2/H_2O reforming.[17,36,37] For instance, García-Diéguez et al.[17a,b] supported Ni/Pt bimetallic NPs on the nanofibrous Al_2O_3 using impregnation or reverse microemulsion methods, and they found that the addition of Pt can promote the formation of NiO, rather than $NiAl_2O_4$, and facilitate its reduction to Ni^0 during the catalyst activation, finally leading to the enhanced activities and the less coke formation for dry reforming of methane. Parizotto et al.[17c] revealed, using *in situ* XANES, that the presence of Pt can initiate the NiO reduction process by rapid dissociation of H_2 and migration of atomic H to the NiO surface by hydrogen spillover, which can maintain Ni in the metallic state under oxidative steam-reforming of methane conditions. It is generally accepted that the presence of Pt can increase reducibility of Ni, no matter during catalyst preparation or reforming test, and improve Ni NP dispersion over inert support because of distinct spillover of H_2 from Pt to Ni. However, the studies on the effects of surface composition and structure of Ni/Pt bimetallic catalyst are to date scarce, although the Pt segregation on the surface of Ni/Pt alloy has already been observed.[36,37]

In our case, the Pt atoms were deposited selectively on the Ni surface with the controlled Pt coverage, and we demonstrated that upon thermal treatment, the Pt surface restructuring takes place, consequently leading to the core-shell bimetallic NPs consisting of the Ni-rich core and Ni/Pt alloy shell. Although the conditions for the thermal treatment is not completely the same as that used for the dry reforming test and the real structures of the bimetallic catalysts under the reaction conditions need to be investigated by *in situ* analysis, we assume that the structures of the bimetallic catalysts are the same under both conditions, which were proven at least partially by the results of XRD (see Figure 3). The attempts to measure the superficial composition of the bimetallic samples after thermal treatment using XPS showed that the superficial composition obtained by XPS is close to the bulk composition obtained by ICP (see Table S1 in Supporting Information), which is inconsistent with that we expected from the proposed structures. It might be because the small particle sizes of the bimetallic samples limit the XPS to distinguish the differences between the bulk composition and the superficial one. Therefore, we suggest that the Pt surface composition of the bimetallic catalysts after thermal treatment is dependent on their initial Pt coverage, i.e., the higher the initial Pt coverage, the higher the Pt composition on the surface after thermal treatment. It is not unexpected that, in our catalyst systems, the intrinsic nature of Pt would contribute to the enhancement of the catalytic activities and suppression of carbon formation because the metal Pt is more active than the Ni for the reforming and it is more resistant toward the carbon formation. Therefore, the presence of more Pt atoms on the surface of the bimetallic catalysts will improve the catalytic activities and inhibit the carbon formation. On the other hand, the presence of Pt on the Ni surface may modify the Ni surface structure electronically and geometrically, which in turn influence the catalytic performance of the catalyst. As illustrated in the case of Ni/Au bimetallic catalyst, deposition of Au on a Ni surface reduce not only the ability to dissociate CH_4 but the stability of the adsorbed C through tuning electronic properties of neighbouring Ni atoms and tailoring ensemble size.[50] We believe that such a mode of combined electronic and ensemble size effects takes effect as well in our Ni/Pt bimetallic catalysts.

In order to further investigate the effects of the surface composition and structure of the bimetallic catalysts on their catalytic activities and carbon formation, a density functional theory (DFT) calculation was carried out. As a matter of fact, a large number of calculations have been to date made for CO_2/H_2O reforming of methane.[51] The activation of the first C–H bond of CH_4 is generally believed to be the rate-determining step although the debates still remain, which is consistent with some experimental results.[49b] However, the recent theoretical studies revealed that the adsorption stabilities and dissociation activation barriers of various reaction intermediates (e.g., CH_x, CO_2, CO, C, H etc.) vary largely with the step (defect) sites on the surface, and the CH species is likely to be most stable CH_x (x= 1,2,3) intermediate and its C–H bond activation is structure sensitive, which is more favourable on the stepped surface than on the flat surface.[8a,52] It has been further suggested that the nucleation of graphite is initiated at the step sites, and the addition of promoters such as S, K and Au can selectively block the step

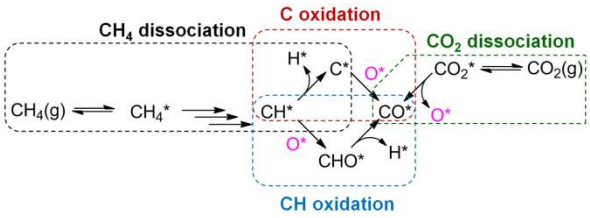

Scheme 2. A schematic diagram for the proposed mechanism for dry reforming of methane.[52]

sites and consequently give rise to a different activation barriers. We believe that the Pt atoms in our bimetallic systems may play the same role as the other promoters like K and Au in the Ni-based catalyst systems. Therefore, we performed a DFT calculation based on a comparable mechanism, in which the oxidation of the CH species including the dehydrogenation (C oxidation) and oxygenation (CH oxidation) pathways dominates the overall reforming reaction and carbon formation, as schematically displayed in Scheme 2,[52] The reaction energies for both pathways were calculated at three different Pt surface coverages. The calculation results showed that as the Pt coverage increases, the reaction energy for the CH dehydrogenation becomes more endothermic, whereas the one for the CH oxygenation becomes more exothermic (see Table S2 in Supporting Information). Since the reaction energies for a given step are linearly correlated to the activation energies through the known Brønsted–Evans–Polanyi (BEP) relations,[53] it is apparent that as the Pt coverage rises, the tendency of the CH oxygenation increases and that of the CH dehydrogenation decreases and consequently results in the less coke formation and higher catalytic activity, which are in agreement with our experimental results.

In conclusion, we develop a SOMC protocol to synthesize the supported Ni/Pt bimetallic NPs with controlled surface composition and structure. The surface restructuring of the bimetallic catalysts upon thermal treatment was investigated using various techniques, demonstrating a structure evolution of the bimetallic NPs from Pt monolayer island-modified Ni NPs to core-shell bimetallic NPs comprised of the Ni-rich core and the Ni/Pt alloy shell. The dry reforming tests showed that the surface modification of Ni-based catalysts by adding the Pt atoms can effectively enhance the catalytic activities and the resistance towards carbon formation. The DFT calculation suggested that the addition of Pt on the Ni surface may facilitate the CH oxidation pathway and inhibit the C oxidation pathway (see Scheme 2), and consequently leads to the enhanced catalytic activity and the suppressed carbon formation as the Pt coverage increases.

Keywords: nickel · platinum · nanoparticles · dry reforming of methane · EXAFS spectroscopy

[1]
[2]
[3]

Table of Contents

[1] a) K. Liu, C. Song, V. Subramani, *Hydrogen and Syngas Production and Purification Technologies*, Wiley, Hoboken, **2009**; b) J. Rostrup-Nielsen, L. J. Christiansen, *Concepts in Syngas Manufacture*, Imperial College Press, London, **2011**.
[2] M. C. J. Bradford, M. A. Vannice, *Catal. Rev.: Sci. Eng.* **1999**, *41*, 1–42.
[3] a) M. F. Mark, W. F. Maier, *Angew. Chem. Int. Ed.* **1994**, *33*, 1657–1660; b) M. F. Mark, W. F. Maier, *J. Catal.* **1996**, *164*, 122–130.
[4] a) J. H. Bitter, K. Seshan, J. A. Lercher, *J. Catal.* **1997**, *171*, 279–286; b) J. H. Bitter, K. Seshan, J. A. Lercher, *J. Catal.* **1998**, *176*, 93–101.
[5] a) J. R. Rostrup-Nielsen, *J. Catal.* **1984**, *85*, 31–43; b) J. R. Rostrup-Nielsen and I. Alstrup, *Stud. Surf. Sci. Catal.* **1988**, *38*, 725–732; c) J. R. Rostrup-Nielsen, *Stud. Surf. Sci. Catal.* **1991**, *68*, 85–101.
[6] M. C. J. Bradford, M. A. Vannice, *Appl. Catal. A* **1996**, *142*, 73–96.
[7] J. R. Rostrup-Nielsen, J. Sehested, J. K. Nørskov, *Adv. Catal.* **2002**, *47*, 65–139.
[8] a) H. S. Bengaard, J. K. Nørskov, J. Sehested, B. S. Clausen, L. P. Nielsen, A. M. Molenbroek, J. R. Rostrup-Nielsen, *J. Catal.* **2002**, *209*, 365–384; b) S. Helveg, C. López-Cartes, J. Sehested, P. L. Hansen, B. S. Clause, J. R. Rostrup-Nielsen, F. Abild-Pedersen, J. K. Nørskov, *Nature* **2004**, *427*, 426–429.
[9] T. Osaki, T. Mori, *J. Catal.* **2001**, *204*, 89–97.
[10] F. Besenbacher, I. Chorkendorff, B. S. Clausen, B. Hammer, A. M. Molenbroek, J. K. Nørskov, I. Stensgaard, Science 1998, 279, 1913–1915.
[11] a) T. Horiuchi, K. Sakuma, T. Fukui, Y. Kubo, T. Osaki, Toshiaki Mori, *Appl. Catal. A* **1996**, *144*, 111–120; b) T. Mori, T. Osaki, T. Horiuchi, T. Sugiyama, K. Suzuki, *Stud. Surf. Sci. Catal.* **1999**, *126*, 365–372.
[12] a) J. Juan-Juan, M. C. Román-Martínez, M.J. Illán-Gómez, *Appl. Catal. A* **2006**, *301*, 9–15.
[13] a) Z. Zhang, X. E. Verykios, *Chem. Commun.* **1995**, 71–72; b) Z. Zhang, X. E. Verykios, *Appl. Catal. A* **1996**, *138*, 109–133.
[14] a) V. M. Gonzalez-DelaCruz, J. P. Holgado, R. Pereñíguez, A. Caballero, J. Catal. 2008, 257, 307–314; b) V. M. Gonzalez-Delacruz, F. Ternero, R. Pereñíguez, A. Caballero, J. P. Holgado, *Appl. Catal. A* **2010**, *384*, 1–9; c) S. Corthals, J. V. Nederkassel, J. Geboers, H. D. Winne, J. V. Noyen, B. Moens, B. Sels, P. Jacobs, *Catal. Today* **2008**, *138*, 28–32.
[15] W. Hallyt, J. H. Bitters, K. Seshans, J. A. Lercher, J. R. H. Ross, *Stud. Surf. Sci. Catal.* **1994**, *88*, 167–173.
[16] a) D. Li, Y. Nakagawaa, K. Tomishige, *Appl. Catal. A* **2011**, *408*, 1–24; b) C. Liu, J. Ye, J. Jiang, Y. Pan, *ChemCatChem 2011*, **3**, 529–541; c) D. L. Trimm, *Catal. Today* **1999**, *49*, 3–10; d) J.-S. Choi, K.-I. Moon, Y. G. Kim, J. S. Lee, C.-H. Kim, D. L. Trimm, *Catal. Lett.* **1998**, *52*, 43–47; e) D. Liu, X. Y. Quek, W. N. E. Cheo, R. Lau, A. Borgna, Y. Yang, *J. Catal.* **2009**, *266*, 380–390; f) J. Zhang, H. Wang, A. K. Dalai, *J. Catal.* **2007**, *249*, 300–310.
[17] a) M. García-Diéguez, I. S. Pieta, M. C. Herrera, M. A. Larrubia, L. J. Alemany, *J. Catal.* **2010**, *270*, 136–145; b) M. García-Diéguez, I. S. Pieta, M. C. Herrera, M. A. Larrubia, L. J. Alemany, *Appl. Catal. A* **2010**, *377*, 191–199; c) N. V. Parizotto, D. Zanchet, K. O. Rocha, C. M. P. Marques, J. M. C. Bueno, *Appl. Catal. A* **2009**, *366*, 122–129; d) D. Liu, W. N. E. Cheo, Y. W. Y. Lim, A. Borgna, R. Lau, Y. Yang, *Catal. Today* **2010**, *154*, 229–236; e) B. Pawelec, S. Damyanova, K.

Arishtirova, J. L. G. Fierro, L. Petrov, *Appl. Catal. A* **2007**, *323*, 188–201; f) Ş. Özkara-Aydınoğlu, A. E. Aksoylu, *Int. J. Hydrogen Energy* **2011**, *36*, 2950–2959.
[18] D. Li, T. Shishido, Y. Oumi, T. Sano, K. Takehira, *Appl. Catal. A* **2007**, *332*, 98–109.
[19] C. Padeste, D. L. Trimm, R. N. Lamb, *Catal. Lett.* **1993**, *17*, 333–339.
[20] N. V. Parizotto, K. O. Rocha, S. Damyanova, F. B. Passos, D. Zanchet, C. M. P. Marques, J. M. C. Bueno, *Appl. Catal. A* **2007**, *330*, 12–22.
[21] J. R. Kitchin, N. A. Khan, M. A. Barteau, J. G. Chen, B. Yakshinskiy, T. E. Madey, *Surf. Sci.* **2003**, *544*, 295–308.
[22] C. A. Menning, J. G. Chen, *J. Chem. Phys.* **2008**, *128*, 164703.
[23] C. A. Menning, J. G. Chen, *J. Power Sources* **2010**, *195*, 3140–3144.
[24] C. A. Menning, H. H. Hwu, J. G. Chen, *J. Phys. Chem. B* **2006**, *110*, 15471–15477.
[25] R. Mu, Q. Fu, H. Liu, D. Tan, R. Zhai, X. Bao, *Appl. Surf. Sci.* **2009**, *255*, 7296–7301.
[26] C. A. Menning, J. G. Chen, *J. Chem. Phys.* **2009**, *130*, 174709.
[27] S. Deckers, S. Offerhaus, F. H. P. M. Habraken, W. F. van der Weg, *Surf. Sci.* **1990**, *237*, 203–212.
[28] J. A. Barnard, J. J. Ehrhardt, H. Azzouzi, M. Alnot, *Surf. Sci.* **1989**, *211–212*, 740–748.
[29] Y. Takasu, H. Shimizu, *J. Catal.* **1973**, *29*, 479–485.
[30] V. R. Stamenkovic, B. S. Mun, K. J. J. Mayrhofer, P. N. Ross, N. M. Markovic, *J. Am. Chem. Soc.* **2006**, *128*, 8813–8819.
[31] S. P. Jeng, P. H. Holloway, C. D. Batich, *Surf. Sci.* **1988**, *193*, L63–L68.
[32] F. Tao, M. E. Grass, Y. Zhang, D. R. Butcher, F. Aksoy, S. Aloni, V. Altoe, S. Alayoglu, J. R. Renzas, C.-K. Tsung, Z. Zhu, Z. Liu, M. Salmeron, G. A. Somorjai, *J. Am. Chem. Soc.* **2010**, *132*, 8697–8703.
[33] Lidong Li, Dalaver H. Anjum, Lu Zhou, Paco V. Laveille, Jean-Marie Basset, US patent, Application number 61917395, **2013**.
[34] a) C. H. Bartholomew, R. B. Pannell, *J. Catal.* **1980**, *65*, 390–401; b) M. Primet, J. A. Dalmon, G. A. Martin, *J. Catal.* **1977**, *46*, 25–36.
[35] a) S. D. Jackson, B. M. Glanville, J. Willis, G. D. McLellan, G. Webb, R. B. Moyes, S. Simpson, P. B. Wells, R. Whyman, *J. Catal.* **1993**, *139*, 207–220; b) R. Barth, R. Pitchal, R. L. Anderson, X. E. Verykios, *J. Catal.* **1989**, *116*, 61–70.
[36] a) Y. Mukainakano, K. Yoshida, S. Kado, K. Okumura, K. Kunimori, K. Tomishige, Chem. Eng. Sci. 2008, 63, 4891–4901; b) B. Li, S. Kado, Y. Mukainakano, T. Miyazawa, T. Miyao, S. Naito, K. Okumura, K. Kunimori, K. Tomishige, *J. Catal.* **2007**, *245*, 144–155.
[37] M. García-Diéguez, E. Finocchio, M. Á. Larrubia, L. J. Alemany, G. Busca, *J. Catal.* **2010**, *274*, 11–20.
[38] K. I. Hadjiivanov, G. N. Vayssilov, *Adv. Catal.* **2002**, *47*, 307–511.
[39] J. Raskó, *J. Catal.* **2003**, *217*, 478–486.
[40] M. Primet, J. M. Basset, M. V. Mathieu, M. Prettre, *J. Catal.* **1973**, *29*, 213–223.
[41] a) Z. Duan, G. Wang, *J. Phys.: Condens. Matter* **2011**, *23*, 475301; b) R. V. hardeveld, F. Hartog, *Surf. Sci.* **1969**, *15*, 189–230.
[42] J. Geng, D. A. Jefferson, B. F. G. Johnson, *Chem. Commun.* **2007**, 969–971.
[43] a) B. Luo, S. Xu, X. Yan, Q. Xue, *J. Electrochem. Soc.* **2013**, *160*, F262–F268; b) W. Wang, Q. Wang, Z. Zhang, J. Nanopart. Res. **2008**, *10*,255–262.
[44] a) R. B. Greecor, F. W. Lytle, *J. Catal.* **1980**, *63*, 476–486; b) A. I. Frenkel, C. W. Hills, R. G. Nuzzo, *J. Phys. Chem. B* **2001**, *105*, 12689–12703.
[45] A. I. Frenkel, *Chem. Soc. Rev.* **2012**, *41*, 8163–8178.
[46] Y. Shu, L. E. Murillo, J. P. Bosco, W. Huang, *Appl. Catal. A* **2008**, *339*, 169–179.
Anatoly I. Frenkel c, Jingguang G. Chen
[47] a) B. Moraweck, A. J. Renouprez, E. K. Hlil, R. Baudoing-Savois, *J. Phys. Chem.* **1993**, *97*, 4288–4292; b) A. N. Mansour, J. W. Cook, Jr., D. E. Sayers, *J. Phys. Chem.* **1984**, *88*, 2330–2334.
[48] E. Choi, S.-J. Oh, M. Choi, *Phys. Rev. B* **1991**, *43*, 6360–6368.
[49] a) J. Wei, E. Iglesia, *J. Phys. Chem. B* **2004**, *108*, 4094–4103; b) J. Wei, E. Iglesia, *J. Catal.* **2004**, *224*, 370–383.
[50] F. Besenbacher, I. Chorkendorff, B. S. Clausen, B. Hammer, A. M. Molenbroek, J. K. Nørskov, I. Stensgaard, *Science* **1998**, *279*, 1913–1915.
[51] a) V. C. H. Kroll, H. M. Swaan, S. Lacombe, C. Mirodatos, *J. Catal.* **1997**, *164*, 387–398; b) L. M. Aparicio, *J. Catal.* **1997**, *165*, 262–274; c) S.-G. Wang, X.-Y. Liao, J. Hu, D.-B. Cao, Y.-W. Li, J. Wang, H. Jiao, *Surf. Sci.* **2007**, *601*, 1271–1284; d) S.-G. Wang, D.-B. Cao, Y.-W. Li, J. Wang, H. Jiao, *Surf. Sci.* **2006**, *600*, 3226–3234; e) Y.-A. Zhu, D. Chen, X.-G. Zhou, W.-K. Yuan, *Catal. Today* **2009**, *148*, 260–267.
[52] Z. Wang, X.-M. Cao, J. Zhu, P. Hu, *J. Catal.* **2014**, *311*, 469–480.
[53] A. Michaelides, Z. P. Liu, C. J. Zhang, A. Alavi, D. A. King, P. Hu, *J. Am. Chem. Soc.* **2003**, *125*, 3704–3705.